

Scale Interactions and Atmospheric Predictability: An Updated Perspective

J. J. TRIBBIA AND D. P. BAUMHEFNER

National Center for Atmospheric Research, Boulder, Colorado*

(Manuscript received 26 March 2003, in final form 2 September 2003)

ABSTRACT

An examination of the scale interactions in predictability experiments is made using the NCAR Community Climate Model Version 3 (CCM3) at various horizontal resolutions ranging from T42 to T170. Both identical-model and imperfect-model twin experiments are analyzed, and they show distinctive differences from the classical inverse cascade picture of predictability error growth. In the identical-model twin framework, error growth experiments using initial errors confined to long and short scales are compared and contrasted. In these cases, error growth eventually asymptotes to an exponential growth of baroclinically active scales. In the imperfect-model twin experiments, errors rapidly disperse from scales technically beyond model resolution to a small amplitude, spectrally uniform distribution of errors in resolved scales. The errors in resolved scales further amplify in a quasi-exponential growth of the baroclinically active scales. Finally, the implications of these growth mechanisms for the necessary resolution in short- to medium-range numerical weather prediction are given under the assumption that the accuracy of current initial state estimates of the atmosphere remain fixed at their present level.

1. Introduction

Thompson (1957), who presented the earliest work on the problem of atmospheric predictability, in addition to establishing the legitimacy of the topic, went on to analyze the relationship between disturbance spatial scale and the growth of errors. Thompson's analysis, using the tools of the statistical theory of homogeneous turbulence (Batchelor 1953), concluded that small amplitude disturbances with spatial scale larger than the radius of deformation would grow in time and errors with scales much smaller than the deformation radius would remain small in amplitude. Thompson's results were useful in the early days of numerical weather prediction for they instilled the hope that accurate predictions on large scales were possible because partially or completely unobserved small scales, whose errors would not grow, would not disrupt the accuracy of the synoptic- or planetary-scale features.

With the advent of more powerful computers in the 1960s, the field of numerical weather prediction flourished, and with this growth, interest in the predictability problem expanded. Lorenz (1963) showed that even low-order representations of atmospheric flow could

have limited predictability. Lorenz (1969) used a closure model of two-dimensional flow to quantify more precisely Thompson's analytic results. Lorenz's numerical model demonstrated the slow inverse cascade of errors from small to large scales, an effect too subtle to be captured in Thompson's early work. Because of the intense interest in predictability generated by the prospects of the Global Atmospheric Research Program (GARP), Lorenz's results were also supported by additional turbulence closure studies. Using improved closure models for the evolution of the energy in wavenumber space, Leith and Kraichnan (1972) verified Lorenz's results, which has led to the accepted picture of the evolution of errors in the wavenumber spectral domain (Fig. 1). This picture combines the elements of Thompson's earliest work with Fjortoft's (1953) theory of spectral energy and enstrophy transfer. In this conventional picture, errors in small scales (high wavenumber) propagate up scale with a constant flux of error energy in spectral space. The main addition to Thompson's work is that small-scale errors grow and eventually contaminate all the skill remaining in larger scale. The implication for weather forecasting is that eventually even the smallest amplitude small-scale error will creep up scale and amplify in time, rendering practical, accurate prediction feasible only for a finite length of time.

A significant outcome of these studies was that attention turned to estimates of this finite time during which one might practically be able to predict the weather at synoptic scales. The results of studies by Sma-

* The National Center for Atmospheric Research is sponsored by the National Science Foundation.

Corresponding author address: Dr. J. J. Tribbia, National Center for Atmospheric Research, P.O. Box 3000, Boulder, CO 80307-3000.
E-mail: tribbia@ucar.edu

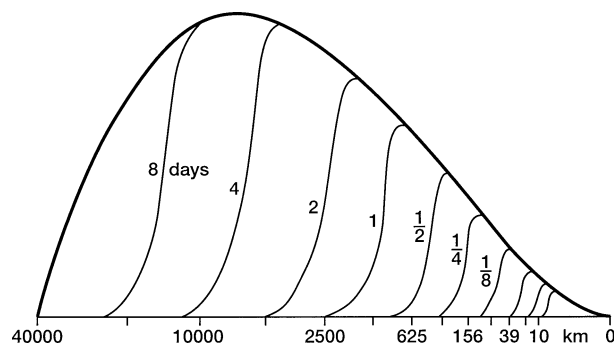


FIG. 1. Growth of errors initially confined to smallest scales, according to a theoretical model Lorenz (1984). Horizontal scales are on the bottom, and the upper curve is the full atmospheric motion spectrum.

gorinsky (1969), Williamson and Kasahara (1971), and later by Daley (1981), gave progressively shorter estimates of the time, beginning with 1 month and culminating at about 10 days. Throughout, the conceptual model of a gradual inverse cascade has remained, and with the extension to three-dimensional flow through the concept of quasigeostrophic (QG) turbulence developed by Charney (1971), the supposition of longtime predictability of planetary scales has remained part of the conventional wisdom of atmospheric predictability.

It should be noted that cascade rates are intimately connected with eddy turnover times in a turbulent fluid, and these are determined by the slope of the energy spectrum. Because a -3 range corresponds to a constant eddy turnover time, one might infer that synoptic- and planetary-scale predictability could be extended indefinitely by sequestering errors to increasingly smaller scales. Note that this would also require that error energy (i.e., magnitude) would necessarily decrease at a rate consistent with the -3 spectral decay law. The classical picture of the inverse cascade of error relies upon the slow constant cascade associated with the spectrally invariant eddy turnover time of the -3 inertial range. Additionally, recent observational studies of the atmosphere have suggested that the enstrophy-cascading -3 spectral range of two-dimensional and quasigeostrophic turbulence is supplanted in the mesoscale by a $-5/3$ range (Gage 1979). The existence of such a range, particularly if it is associated with an inverse cascade of energy as speculated by Gage (1979) and Lilly (1983), could have important predictability ramifications because it would imply that even microscale errors (just above the molecular dissipation scale) could impact synoptic and subsynoptic scales in a finite time. Although the questions raised by the possibility of an energy-cascading $-5/3$ range in the mesoscale are important, these questions are beyond the resolution of the synoptic-scale predictability focused upon in the works cited above and, indeed, beyond the resolution of the numerical experiments to be reported here.

With renewed interest in observational strategies

sparked by programs such as the North American Observing System (NAOS), the U.S. Weather Research Program (USWRP), and the Navy Predictability Directed Research Initiative, the quantification of propagation rates of error variance across scales and of scale interactions is extremely relevant. Such estimates will permit a rational choice of observational strategy that may be targeted to allow the accurate prediction of phenomena of a chosen scale. Since it has been two decades since such quantities were computed in the works cited above, and forecast and climate models have continued to develop over that time, this work will reexamine the questions of interscale influence in predictability error growth. In the following sections we develop an experimental design that can test the validity of this conventional wisdom regarding scale interactions and predictability error growth in large and small scales. We also test directly the effects of scale limitations of errors and unresolved scales and processes to examine anew the relevance of QG turbulence ideas in the context of a modern atmospheric GCM, useful both for numerical weather prediction and climate simulation.

2. Experimental design

There are two components of the experimental design that are to be specified: the models used and the types of initial errors specified. The interrelationship of these two components define each experiment. The numerical model used in these experiments is the NCAR Community Climate Model Version 3 (CCM3; Kiehl et al. 1998), which has well-documented capabilities as an atmospheric climate model and a medium-range forecast tool (Shukla et al. 2000; Baumhefner et al. 2003, unpublished manuscript; see also the appendix). The model is run at a range of horizontal resolutions, from T42 to T170. The initial data for the atmospheric model are taken from the National Centers for Environmental Prediction (NCEP) operational analysis, with experiment dates taken from the boreal winter of 1995/96.

In experiments with nonzero initial errors, the error fields are random realizations with a spatial spectrum that matches an estimate of analysis errors (Mullen et al. 2003, unpublished manuscript). This estimate is obtained for the time-mean spectral distribution of the difference between the NCEP–National Center for Atmospheric Research (NCAR) and the European Centre for Medium-Range Weather Forecasts (ECMWF) reanalysis for the boreal winters of the 1990s. Because the small scales in analyses—those with two-dimensional wavenumber beyond $n = 30$ —have little accuracy, the estimated variance of errors in these scales can easily be greater than the (control) variance in these scales on a given day. To avoid the problem of an unphysical spectrum in perturbed realizations, when the spectrum of perturbations intersects the unperturbed spectrum, the perturbations are tapered to the spectral shape of the unperturbed analysis (Fig. 2a). The spectral

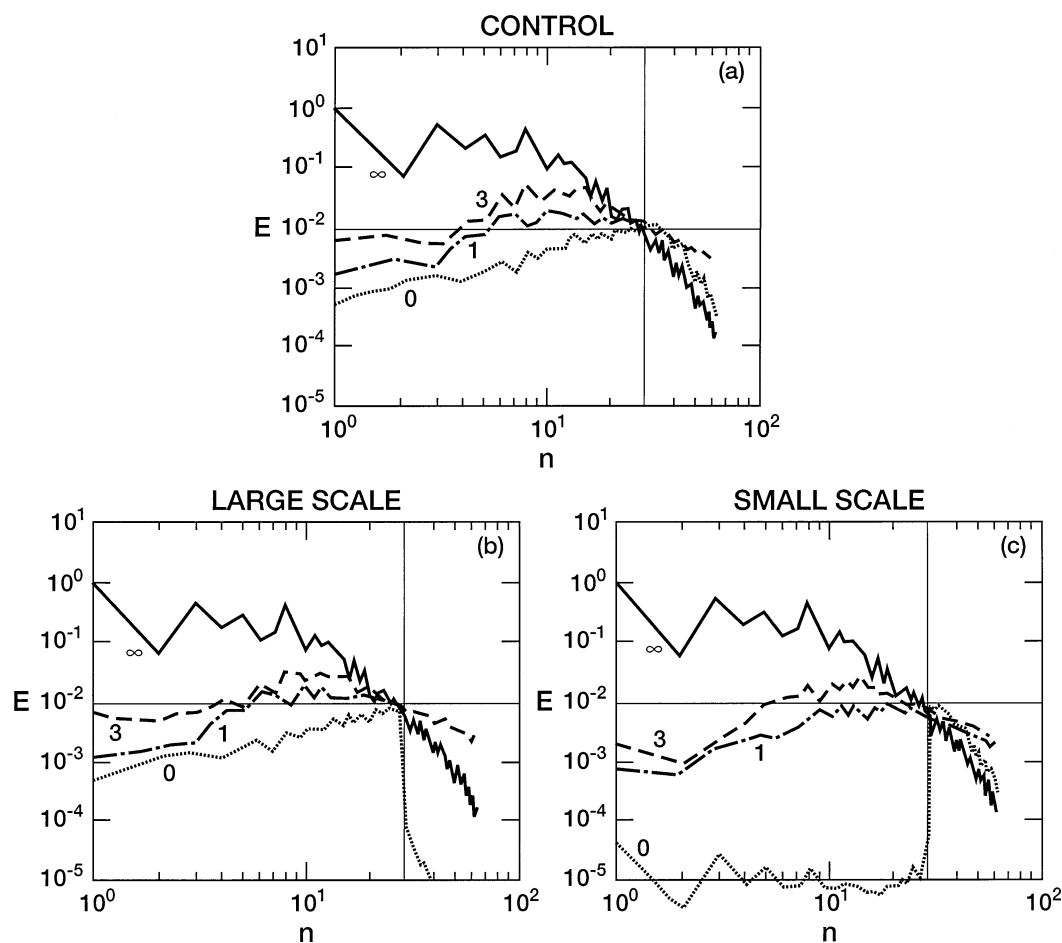


FIG. 2. Kinetic energy spectrum for 500 mb plotted for 2D wavenumber n indicated on abscissa. Amplitude of each wavenumber is on ordinate. Solid line is the spectrum of full field, and dotted (day 0), dashed-dotted (day 1), and dashed lines (day 3) are the spectrum of the difference fields from ensemble members (a) full perturbation in all scales, (b) perturbations only in wavenumber ≤ 30 , and (c) perturbations only in wavenumber > 30 .

shape of these initial condition perturbations is quite different from the dynamical perturbations used by the operational centers, NCEP and ECMWF. There is a slowly increasing magnitude of perturbation difference variance at all wavenumbers out to the intersection of the perturbation kinetic energy spectrum with the total (control) kinetic energy spectrum. The singular vector perturbations used by ECMWF are smaller by an order of magnitude and are more localized. The bred vector perturbations used at NCEP have a strong spectral peak at wavenumber 8 that tapers off toward smaller and larger wavenumbers (D. P. Baumhefner et al. 2003, unpublished manuscript).

The first set of experiments described below will be what is termed identical-model twin experiments. In these numerical integrations, a fixed resolution model (T63) will be initialized with the observed analyses for a single day and integrated forward in time. This integration will be termed the control or (pseudo) truth run. Perturbed integrations are obtained in a manner similar to what is done operationally in ensemble pre-

diction, except that the perturbations will be generated using the analysis error simulator described above. These experiments will give an estimate of the rate of error growth due to imperfections in the current analysis system. Variations of this experiment will band limit the initial error spectrum in order to allow an analysis of the speed at which errors in particular scale ranges produce broadband forecast errors. These experiments will also permit an identification of the spatial scales of errors most deleterious to a prediction of a given scale.

The second set of experiments are imperfect- or fraternal-model twin experiments in which the model used as truth or control differs from the model that is used for the predictability experiments. In our case, the control integration is taken from a T170 integration. In the experiments below, we will examine the error growth in the T42, T63, T106, and T170 versions of CCM3 in cases in which the initial condition error is quite small. The dominant source of error is the difference in resolution between the high-resolution control and the coarser-resolution forecast models. These experiments

will allow us to analyze the resolution beyond which it is no longer effective to increase resolution given the current accuracy of analyses and rate of leakage of errors from unresolved to resolved scales if the objective is forecasting synoptic-scale weather.

3. Experimental results

a. Perfect-model twin experiments

In the first group of experiments, we compare the growth of errors that have a full range of spectral variability with those for which errors have been suppressed in broad wavenumber bands. A control integration and nine perturbation runs were made from NCEP's operational analysis for 8 January 1996 at 1200 UTC. In the first experiment, which depicts the growth of unfiltered error shown in Fig. 2a, the spectral evolution of the error energy is shown at days 0, 1, and 3. One can note that despite the qualitative similarity of the initial error energy spectra in Fig. 2a, and the error spectrum at day 1 in Fig. 1, the spectral structure of the subsequent growth of error energy differs considerably in these two figures. In particular the fastest growing band of energy in Fig. 2a is the range of wavenumbers between 6 and 20, while the higher wavenumbers amplify at the same rate as this peak. In Fig. 1, however, the error growth is tied to the saturation scales, and the spectral evolution of the error progresses through the up-scale evolution of the saturation scale. The effect of synoptic-scale growth inducing growth at small scales can be seen more clearly in the experiment examining near-perfect initial conditions for the small scales (two-dimensional wavenumber, n , greater than 30) and typical error in the large scales (two-dimensional wavenumber less than 30). From the error growth shown in Fig. 2b, there is very little utility in accurately specifying small scales. Growth of error in the synoptic scales will almost immediately induce errors in the small scales, and after 3 days the spectral content of the errors will be almost identical to that which would have occurred if the small scales were as inaccurately specified as is typical using current analyses practices.

A different picture emerges if errors in the largest scales are nearly eliminated. In this case there is a lag in time of the growth of errors in the large scale reflective of the necessity of injecting errors through a cascade process into the baroclinically active scales. As opposed to the traditional paradigm of predictability error growth shown in Fig. 1, once errors reach the baroclinically active band (6–20), the errors amplify at an exponential rate. Further growth resembles that in Fig. 2a, with a time delay of about 1 day. The logical consequence of this experiment is that there is some benefit to the accurate specification of the large- to synoptic-scale structures in the initial state, but typical analysis errors in wavenumbers 30 through 63 is sufficient to

limit that benefit to approximately a day of extra predictive skill.

A complementary view of the error growth in these band-limited experiments can be seen by comparing the z500 error fields for one pair of forecasts within the ensemble. Figures 3a–c show the initial errors in geopotential height at 500 mb in the standard (full spectrum) and in the large and small-scale band-limited experiments. One can note in these fields the influence of continentality on the simulated analysis error fields, with high accuracy over the continents with a more dense observing system and less accuracy over the less well-sampled oceanic regions. Examining these fields after 1 day (Figs. 4a–c), one notes that the structure and magnitude of the full spectrum and large-scale error field resemble each much more closely than the (initially) small-scale field. This behavior continues out to 3 days (Figs. 5a–c), where it is clear that the (initially) high-pass error field is lagging in magnitude by at least 1 day. The scale decomposition of the growth in the first 24-h period shows the nearly linear, independent behavior of error growth in each band.

Three individual examples of local error growth are worth noting. We first examine error in the large scale (LS) at 45°N, 160°W (Fig. 3a, see black dot in eastern Pacific). Decomposition of the initial error shows most of the amplitude (45 m) in the LS and only 10 m in the small scale (SS). After 1 day (Fig. 4), the total error at 51°N, 150°W has grown from 55 to 85 m, with the partition of absolute magnitude dominated by the LS (75 m). In this case, almost all the growth occurred in the local LS. The second example is located at 40°N, 62°W (see black dot in the western Atlantic), where the initial error is small in magnitude (25 m). Figures 3b and 3c show the partition of error to be +10 m in the SS and approximately +15 m in the LS. The primary error growth after 1 day at 43°N, 58°W (Fig. 4) has occurred in the SS (75 of 85 m total), and only a small fraction is attributable to the LS. Once again the dominant local scale, in this case the SS, provides most of the growth in perturbation amplitude. The final example, which illustrates a cancellation of error between the two scales, is located at 42°N, 143°E. Figures 3b and 3c show initial error of opposite sign (LS = −10 m and SS = +25 m). The resulting growth after 24 h reveals very little total growth, but the LS grew to −50 m while the SS grew to 35 m. Even though the individual scales grew significantly in amplitude, the total error did not grow substantially. In general, error growth in the first 24 h appears to be in situ or advected growth of existing scales and not scale interaction. By 72 h (Fig. 5), the nonlinear aspects have apparently become more active, and considerable scale interaction takes place.

b. Imperfect-model twin experiments

As noted above, the control or (pseudo) truth for the imperfect-model twin experiments is an integration of

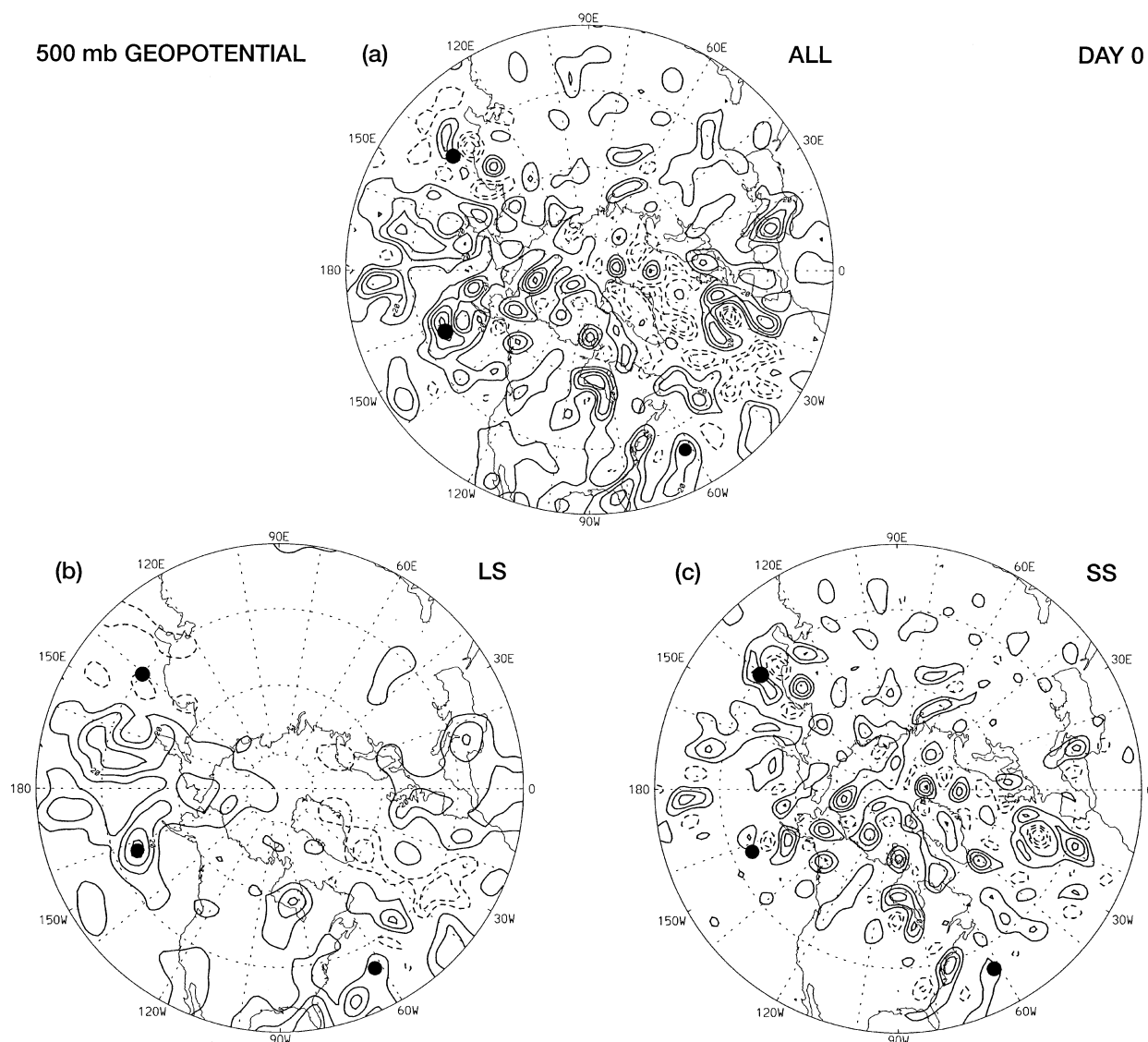


FIG. 3. Difference field of 500-mb geopotential at initial time for one pair of ensemble members shown in Fig. 2. Contour interval is 10 m, solid indicates positive difference, dashed indicates negative difference, and black dots are locations referred to in text.

the T170 version of CCM3. In these experiments we consider T42, T63, and T106 versions of CCM3 with initial states as near as possible in the scales resolved in each individual model to that of the T170 model. A major complication in eliminating initial data discrepancies involves the significantly different topographic fields used in each version of the model. (Although in principle, with a spectral transform model, one might expect the resolved topography to be identical for each model, this is not the case. The additional smoothing and filtering used to minimize Gibbs effects near the continents make, for example, the T42 truncation of the T170 topography significantly different from the topography used in the T42 version of the model.) It also should be noted that the fourth-order hyperviscosity used in each version was the standard value utilized in

climate simulation mode and tuned specifically for each horizontal resolution.

Since the purpose of these experiments was to quantify in a realistic model the cascade rate of unresolved variables into resolved errors, the resolved topographic differences were an undesirable difference in the numerical models. In all imperfect-model twin experiments, that is, in all truncations of the model reported on in this section, then, the topographic field was completely flattened. The T170 version of the model was then initialized with the observed analysis from the NCEP–NCAR reanalysis, using the analysis error simulator to synthesize the initial fields beyond the resolution of the analysis in a manner consistent with the small-scale spectral slope of the analysis. The fields were then subjected to nonlinear normal-mode initial-

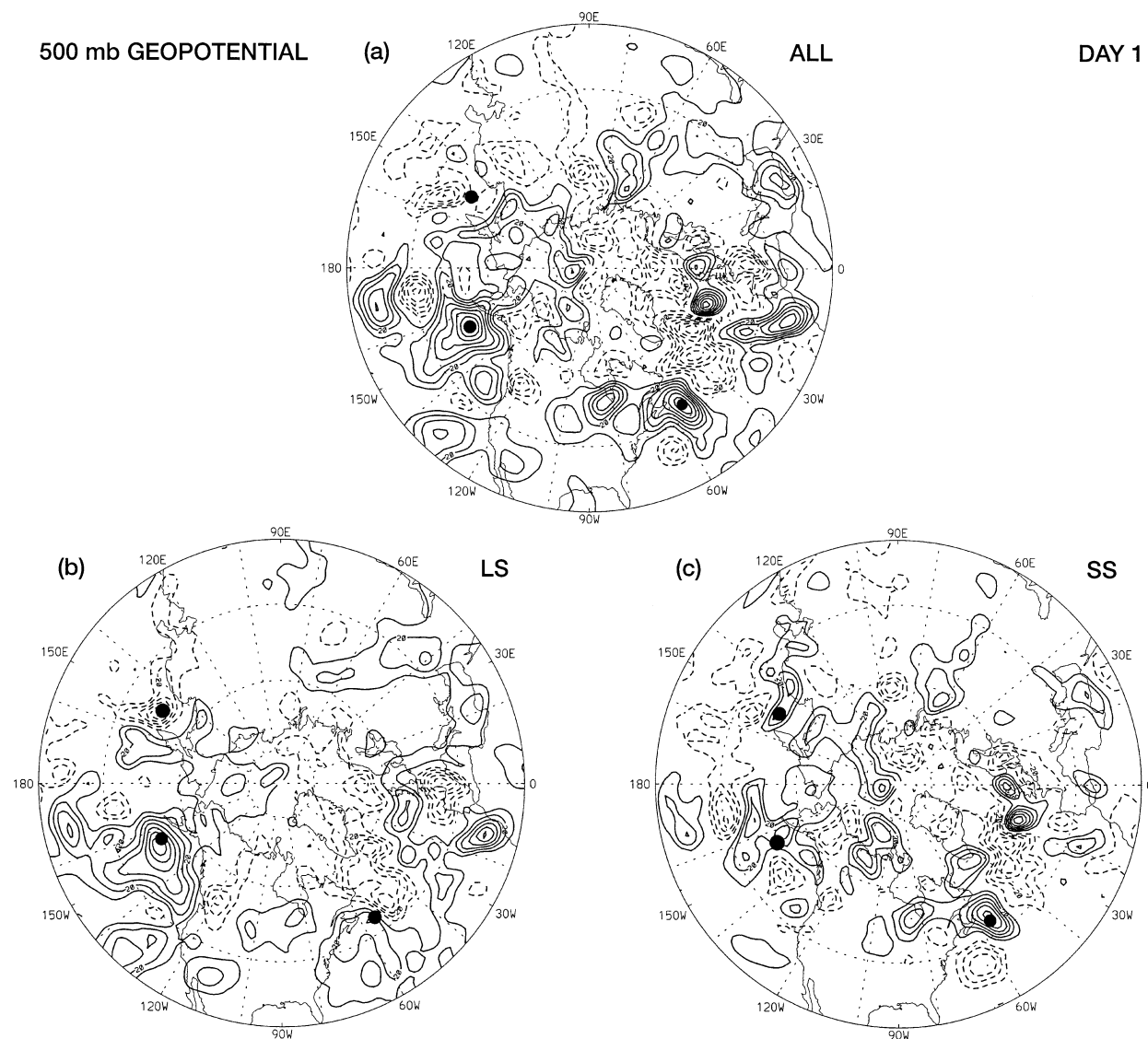


FIG. 4. Same as Fig. 3, but for 1-day forecast.

ization and integrated forward in time for 2 days to allow further adjustment to the spinup shock effects of the altered topography. The 48-h T170 fields were truncated to the specific resolution of each model. Ten initial states spaced throughout the boreal winter of 1995/96 were used to provide 10 individual T170 control integrations.

Despite the elaborate attempts to eliminate all discrepancies between the resolved initial states, a small residual difference remained of order 10^{-7} in the kinetic energy metric. The reason for this is apparently a dry convective adjustment prior to the first model time step. Figures 6a–c show the control spectrum and the error energy spectrum as a function of time for 0.25 to 4.00 days for the truncated models. The most remarkable aspect of these figures is the very rapid error growth within the interval of 0 and 0.25 days. Note that at the

initial time the errors are so small in magnitude that they would be plotted below the range of energies shown in the figure. At the end of 6 h the errors have grown by six–seven orders of magnitude. After the first quarter day, the error growth continues in a manner similar to that displayed in the perfect-model twin experiments. With a full spectrum of errors, the growth is most rapid in the synoptic–baroclinically active range, and amplification of errors is exponential in this range, with an error doubling time of less than 2.00 days (1.60 days).

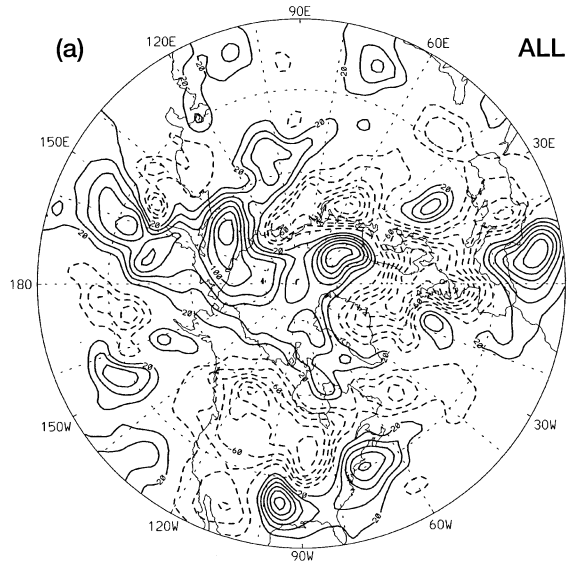
Not surprisingly, the greatest difference is displayed with the T42 truncation. At 6h, the T42 errors are an order of magnitude larger than those of the T106 integration. By day 2, the T42 errors are commensurate with those of the T106 integration at day 4. All three truncations exhibit a similar spectral shape and growth pattern, with the maximum amplitude error initially be-

500 mb GEOPOTENTIAL

(a)

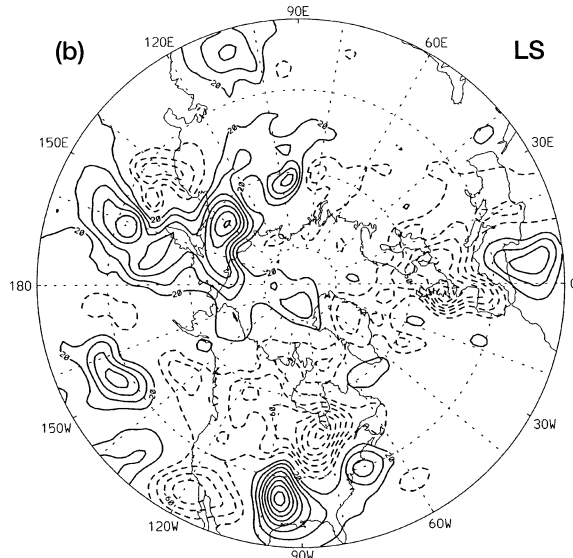
ALL

DAY 3



(b)

LS



(c)

SS

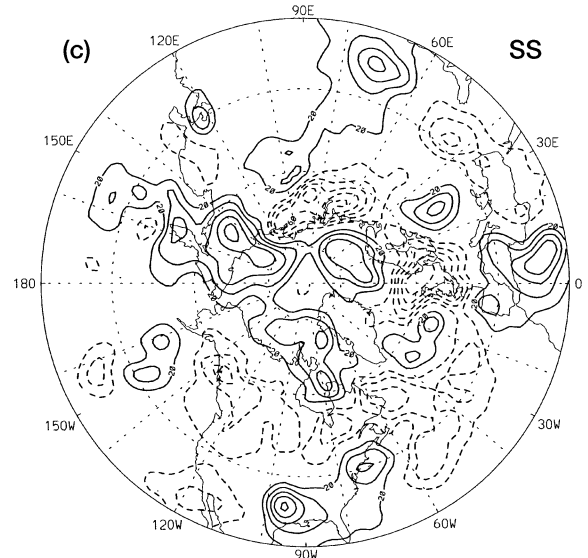


FIG. 5. Same as Fig. 3, but for 3-day forecast and with a contour interval of 20 m.

KINETIC ENERGY SPECTRA

500 mb

T42

T63

T106

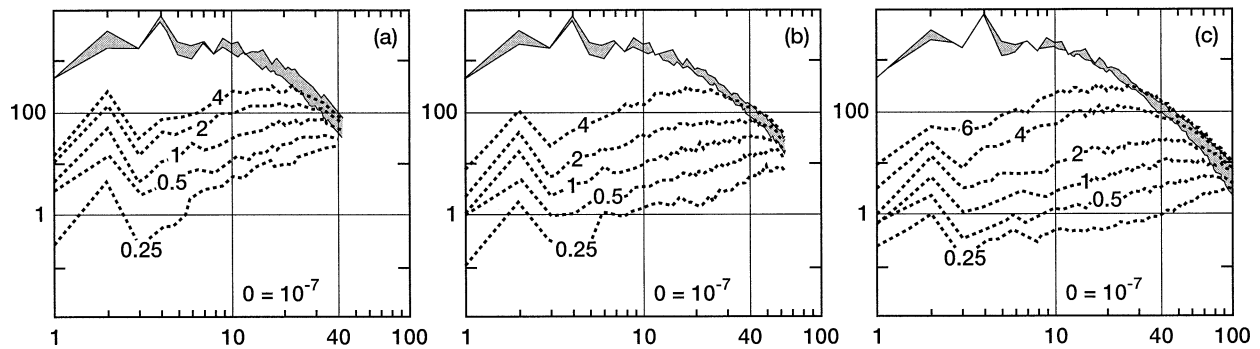


FIG. 6. Same as Fig. 2, but for three different model truncations. Gray shading shows full spectrum change in 5 days (gray indicates reduction in energy). Dashed line labeled by time in days shows growth in error as measured by differencing the forecast with T170 run (truth): (a) T42, (b) T63, and (c) T106 model.

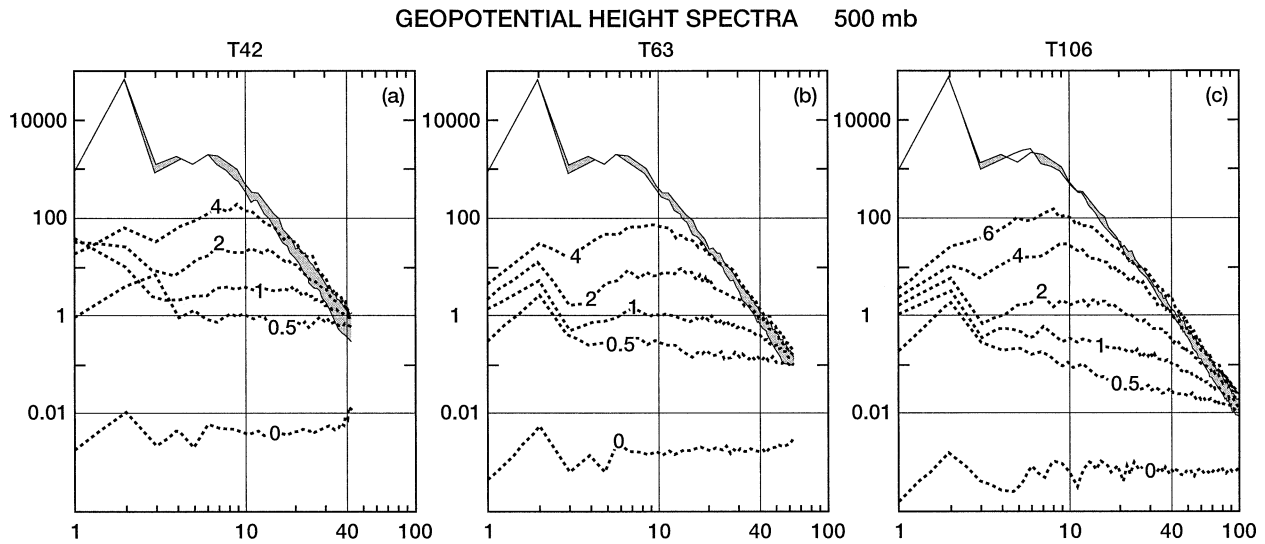


FIG. 7. Same as Fig. 6, but for 500-mb geopotential.

ing near the respective spectral truncation and shifting to the most unstable waves (6–20) at the end of the experiment. Saturation of error energy at $n = 25$ occurs at 4 days for the T42 results, while the higher-resolution integrations do not reach $n = 25$ saturation at day 4.

4. Discussion

There are two aspects of the above experiments that merit further discussion, particularly in contrast to the conventional picture of predictability error growth in the spectral domain. The first relates to the mechanism of predictability error growth, a topic considered in detail in Baumhefner and Errico (2003, manuscript submitted to *Bull. Amer. Meteor. Soc.*). As stated above, the conventional picture of error growth relates to an inverse cascade of errors from smaller to larger scales via the (nonlinear) inertial terms in the hydrodynamic equations. This mechanism depends upon a saturation of error energy in the smaller scales and transfer of “excess” to the locally nearest larger scales of motion. This is particularly true in the depiction of error growth in closure models but is inherently built into the two-dimensional and QG turbulence view of an inverse cascade. Our results above allow a different interpretation that emphasizes the importance of the potential exponential growth of errors in the synoptic scales. This picture is more easily seen in the examination of the imperfect-model twin experiments in which there is a longer time for the exponential growth to occur, since the initial error is smaller in magnitude. It is also more easily seen in the geopotential height spectrum, which has steeper spectral slope. In Fig. 7, a fuller delineation of the temporal growth of the error spectrum for the T42, T63, and T106 imperfect-model twin experiments is shown for the 500 mb geopotential height field. This clearly shows a period of exponential growth in the

synoptic scales in the interval between 0.5° and 3.0° days. (This can be inferred from the linear growth with time of the peak in the spectrum plotted on a logarithmic scale.)

In our alternative view the inverse cascade becomes of lesser importance than in the traditional view. The primary role of the inverse cascade is to seed disturbances in the baroclinically active region of the spectrum. Once in the synoptic scales, the errors organize within the synoptic structures and amplify, extracting energy from the large-scale background flow, not the smaller scales. Such a process is similar to the depiction of growth in singular vectors used at ECMWF (Palmer et al. 1994) for ensemble prediction. In the case of the fastest growing singular vectors, a rapid amplification and up-scale transfer of energy occurs, after which a slower exponential growth occurs that is locked into synoptic-scale flow features. The exponential growth is thus preceded by a seeding of synoptic-scale variance corresponding to the structural evolution of singular vectors from small- to synoptic-scale perturbations.

The second result in need of further elucidation is the very rapid growth and transfer of error energy in the imperfect-model twin experiments. The rapid amplification of errors in this manner has been noted previously by Williamson and Kasahara (1971), once again in the context of the imperfect-model twin framework. Williamson and Kasahara relate this superexponential growth phase to the presence of threshold parameterizations of atmospheric processes, for example, dry convective adjustment and large-scale condensation. This is also the case in our experiments where the presence of gridpoint discrepancies between the initial fields at various resolutions combined with threshold physics can initiate large diabatic tendency differences and consequent spectrally white error growth.

5. Conclusions

Herein we reiterate the main points of the paper and draw some conclusions as to the meaning of these results for numerical prediction of synoptic-scale phenomena. The first main result of this paper is the modification of the traditional view of error growth in the spectral domain. The evidence shown above suggest that a critical aspect of error predictability error growth is the excitation and amplification of structures within the baroclinically active band of wavenumbers 6–20. Thus, in the experiments using band-limited error fields, errors that had amplitude only in the synoptic and larger scales grew at a near-identical rate to errors that were not band limited. Conversely, errors that were band limited in scales shorter than synoptic scales required additional time for the inertial cascade processes to seed the baroclinically active regions of the spectrum before growth could proceed. In the experiments shown where the cut-off wavenumber is 30, the delay in error growth due to the necessity of inertial cascade seeding was between 1 and 2 days.

The main result of the experiments in which lack of resolution was the only source of error (i.e., the imperfect-model twin experiments) was that such model errors rapidly led to errors that were spectrally white in space and of significant amplitude in about 6 h. Because such errors are associated with the parameterized physical processes in the model, one might question the physical propriety of such an effect in the real atmosphere, especially at the scales resolved by the global model. Indeed, it is likely true that threshold phenomena do not exist when considering the average (parameterized) behavior of the atmosphere at scales of 300 km and greater. However, since all current numerical climate and prediction models utilize such parameterizations, the error source terms computed are real errors in the algorithmic formulation of prediction/climate models.

The implication of the band-limited results for prediction and observing strategies may seem at first glance limited because no observing/analysis strategies are formally band limited in their error characteristics. However, one interpretation of these results might be the distinction between oceanic and continental observations and the utility of the dense observing network over land. Our results suggest that, if the coarse-resolution observing network is insufficiently accurate in specifying the synoptic scales, the utility of accurate small-scale information is quite small. Alternatively, the prediction of synoptic and larger scales does not suffer exorbitantly from the inaccurate specification of small scales. Yet another interpretation might use the theory of geostrophic adjustment (Rossby 1937; Obukhov 1949), which suggests that, for spatial scales larger-smaller than the Rossby radius of deformation, the balanced component of the flow is nearly identical to the geopotential–vorticity field to identify small scales with

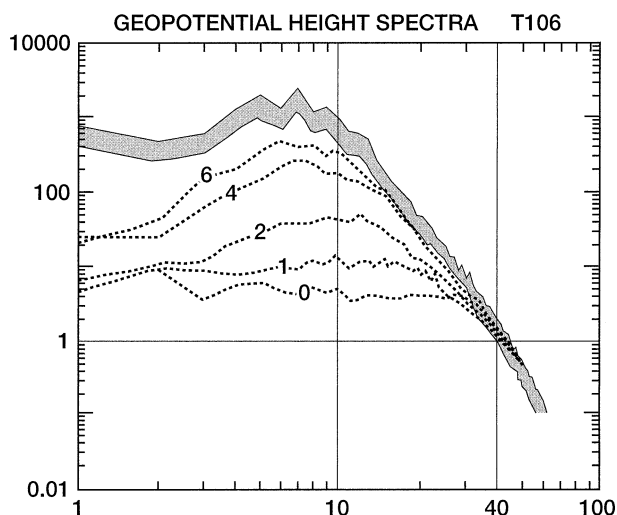


FIG. 8. Same as Fig. 7, but for ensemble dispersion error growth from errors specified in the initial condition. Gray shading indicates σ difference from total 2σ saturation.

velocity measurements and large scales with observations of temperature and pressure.

With respect to the broader implications of the imperfect-model twin experiments, conclusions may be drawn as to the impact of increasing resolution of numerical models focused on predicting the synoptic scales. Note that the analysis below is only valid for dynamical weather elements such as wind and temperature and would be invalid for more-difficult-to-predict elements such as precipitation or vertical motion. From Figs. 6a–c, one can see that after 2 days the errors in synoptic scales are an order of magnitude smaller in the T63 experiments as compared to the T42 experiment. Similarly, there is an order of magnitude increase in comparing T63 to T106. The major implication of this result is that, in going from T42 to T63, one gains a full day of predictability of the synoptic scales. As before, 1 full day of predictability can be gained in going from T63 to T106. This is, of course, in the idealized circumstance of no initial state error. Perhaps the most fundamental application of these experimental results is the comparison of error growth due to truncation and errors in the initial conditions. For the initial error experiments, we use the T106 model and the 10 cases mentioned previously. We determine the average ensemble dispersion by creating nine perturbed initial state ensemble integrations using the analysis error simulator. The error spectra at days 0, 1, 2, 4, and 6 are shown in Fig. 8. Comparing Figs. 7 and 8 reveals a similar behavior with respect to spectral error growth; however, the level of amplitude for each day is higher in the analysis uncertainty cases.

The comparison is summarized in Fig. 9, where the 24-h error growth is plotted for each model truncation along with the error growth due to initial condition (IC) uncertainty from Fig. 8. Even for the coarse resolution

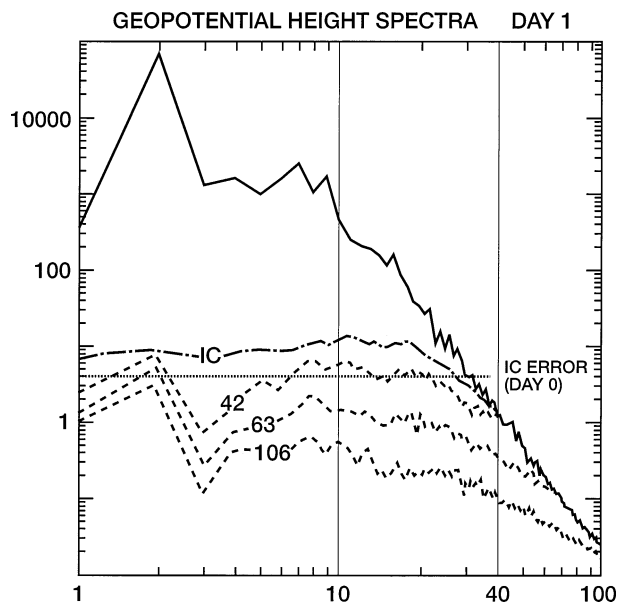


FIG. 9. The 500-mb geopotential height spectra for day 1 forecasts. Solid line indicates full saturated spectra (random maps at day 1), dashed lines from Fig. 6 for various labeled truncations, dotted-dashed line for Fig. 8 at day 1, and dotted line indicates estimate of initial level of uncertainty in analyses.

of T42, the truncation error growth has not exceeded the growth from IC sources. In fact, the T63 and T106 spectra are more than an order of magnitude smaller. This is equally true for forecasts out to at least 4 days. Clearly, the information content of scales below T63 will not overcome the errors in the full spectrum of the initial state. Therefore, if our estimate of initial error/uncertainty is correct, and, if model error is not a significant component of forecast error, the model resolution necessary for accurate forecasts of large-scale baroclinic systems need not be greater than T106. The analysis error must be reduced by a full order of magnitude before a resolution increase beyond T106 is necessary. It should be noted that the above conclusions can only be drawn under the assumption of a negligible impact of resolution on model errors.

The main intent of this work is to give a critical reappraisal of the nature of the scale interaction mechanisms associated with the growth of perturbations in a current state-of-the-art forecast model. While the general nature of predictability error growth has been reexamined in light of improvements in the forecast skill, giving updated estimates of error doubling times and the consequent limit of predictability, comparable updates of the implication of the improved forecast skill on the scale interaction aspects of error growth have not been forthcoming. Given that the forecast performance at planetary and synoptic scales is significantly improved in present global models compared to those models used for NWP in the 1970s and 1980s, it is timely to investigate these mechanisms, particularly when

questions regarding the scale resolution requirement of the next-generation observing system are currently being debated. The main results of our reexamination of spectral error growth in the NCAR CCM3 are as follows:

- 1) For initial errors that have amplitude and spatial structure similar to that of the current-day analysis methods, the growth of errors is more akin to exponential growth of amplifying baroclinic disturbances with a spectral peak in synoptic scales (wavenumbers 10–20) than an inverse cascade.
- 2) Spectrally band-limited initial error distributions rely on a cascade mechanism of error growth only to seed errors into the baroclinically active wavenumbers after which error growth occurs via the exponential amplification mechanism referred to above.
- 3) Highly nonlinear threshold physical parameterizations effect a rapid impact of errors from unresolved scales in the differing-resolution imperfect-model twin experiments performed.
- 4) This rapid transfer of errors across scales seeds baroclinically active scales efficiently and allows us to estimate the optimal, cost-effective resolution for the prediction of synoptic-scale weather as close to T106.

Acknowledgments. The authors wish to thank D. Williamson for providing the various resolution versions of CCM3 used in this study; T. Mayer for the software for analyzing the numerical experiments; and J. Anderson, G. Branstator, A. Kasahara, and R. Saravanan for providing constructive reviews. This work was partially supported by Grant N00014-99-1-0017 from the U.S. Office of Naval Research.

APPENDIX

Skill of the NCAR CCM3 as a Short-Range Forecast Model

The purpose of this appendix is to document the skill of the NCAR CCM3 as a short-range forecast model. A more detailed exposition is given in Baumhefner and Errico (2003, manuscript submitted to *Bull. Amer. Meteor. Soc.*). For the short- to medium-range predictability studies performed herein, it suffices to show a standard skill measure. In Fig. A1 from Baumhefner and Errico, the variance skill score averaged over 10 winter cases using the NCAR CCM3 at T106 resolution is shown in the curve marked control. Also shown is the mean skill of a 10-member ensemble of forecasts using the synthetic analysis error perturbation technique discussed in section 2, along with the dispersion of the ensemble about the ensemble mean. As can be noted from the figure, the error variance of the control forecast crosses the climatological variance (σ^2) (equivalent to an anomaly correlation score of 0.5) at approximately

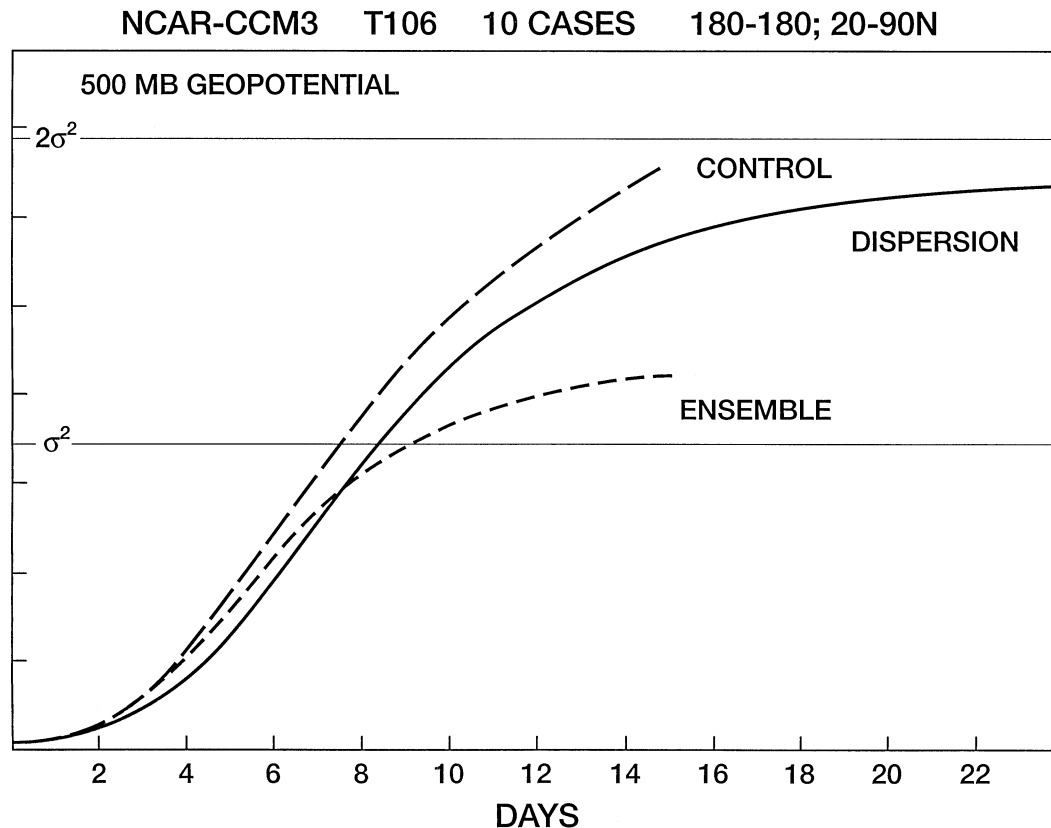


FIG. A1. The control forecast error variance, ensemble dispersion, and error variance of the ensemble mean computed for the CCM3 for 10 cases during one season for the 500-mb height, measured poleward of 20°N and presented as in Fig. 1. The value of σ^2 is the variance of corresponding analyses during this season, equal to 13 800 m².

day 7. This is within 1 day of the comparable crossing time for the operational ECMWF and NCEP forecast models and thus gives validity to the NCAR model as a reasonable tool to use in forecast/predictability studies.

REFERENCES

- Batchelor, G., 1953: *The Theory of Homogeneous Turbulence*. Cambridge University Press, 197 pp.
- Charney, J. G., 1971: Geostrophic turbulence. *J. Atmos. Sci.*, **28**, 1087–1095.
- Daley, R., 1981: Predictability experiments with a baroclinic model. *Atmos.–Ocean*, **19**, 77–89.
- Fjortoft, R., 1953: On changes in the spectral distribution of kinetic energy for two-dimensional non-divergent flow. *Tellus*, **5**, 225–230.
- Gage, K. S., 1979: Evidence for a $k^{-5/3}$ law inertial range in mesoscale two-dimensional turbulence. *J. Atmos. Sci.*, **36**, 1950–1954.
- Kiehl, J. T., J. J. Hack, G. B. Bonan, B. A. Boville, D. L. Williamson, and P. J. Rasch, 1998: The National Center for Atmospheric Research Community Climate Model: CCM3. *J. Climate*, **11**, 1131–1149.
- Leith, C. E., and R. H. Kraichnan, 1972: Predictability of turbulent flows. *J. Atmos. Sci.*, **29**, 1041–1052.
- Lilly, D. K., 1983: Stratified turbulence and the mesoscale variability of the atmosphere. *J. Atmos. Sci.*, **40**, 749–761.
- Lorenz, E. N., 1963: Deterministic nonperiodic flow. *J. Atmos. Sci.*, **20**, 130–141.
- , 1969: Predictability of a flow which possesses many scales of motion. *Tellus*, **21**, 289–307.
- , 1984: Estimates of atmospheric predictability in the medium range. *Predictability of Fluid Motions: A.I.P. Conference Proceedings*, No. 106, American Institute of Physics, La Jolla Institute, 133–140.
- Obukhov, A. K., 1949: On the question of the geostrophic wind. *Izv. Acad. Sci. SSSR, Ser. Geogr.-Geofiz.*, **13**, 281–306.
- Palmer, T. N., R. Buizza, F. Molteni, Y.-Q. Chen, and S. Corti, 1994: Singular vectors and the predictability of weather and climate. *Philos. Trans. Roy. Soc. London*, **A34**, 459–475.
- Rossby, C. G., 1937: On the mutual adjustment of pressure and velocity in certain simple current systems, 1. *J. Mar. Res.*, **1**, 15–28.
- Shukla, J., and Coauthors, 2000: Dynamical seasonal prediction. *Bull. Amer. Meteor. Soc.*, **81**, 2594–2606.
- Smagorinsky, J., 1969: Problems and promises of deterministic extended range forecasting. *Bull. Amer. Meteor. Soc.*, **50**, 286–311.
- Thompson, P. D., 1957: Uncertainty of the initial state as a factor in the predictability of large scale atmospheric flow patterns. *Tellus*, **9**, 275–295.
- Williamson, D. L., and A. Kasahara, 1971: Adaptation of meteorological variables forced by updating. *J. Atmos. Sci.*, **28**, 1313–1327.